



Cargo properties play a critical role in myosin Va-driven cargo transport along actin filaments

Arthur J. Michalek^{a, **}, M. Yusuf Ali^{b, *}

^a Department of Mechanical and Aerospace Engineering, Clarkson University, Potsdam, NY, 13699, USA

^b Department of Molecular Physiology and Biophysics, University of Vermont, Burlington, VT, 05403, USA

ARTICLE INFO

Keywords:
Myosin Va
Cargo transport
Tether force
Rigidity
Stochastic model

ABSTRACT

High-resolution experiments revealed that a single myosin-Va motor can transport micron-sized cargo on actin filaments in a stepwise manner. However, intracellular cargo transport is mediated through the dense actin meshwork by a team of myosin Va motors. The mechanism of how motors interact mechanically to bring about efficient cargo transport is still poorly understood. This study describes a stochastic model where a quantitative understanding of the collective behaviors of myosin Va motors is developed based on cargo stiffness. To understand how cargo properties affect the overall cargo transport, we have designed a model in which two myosin Va motors were coupled by wormlike chain tethers with persistence length ranging from 10 to 80 nm and contour length from 100 to 200 nm, and predicted distributions of velocity, run length, and tether force. Our analysis showed that these parameters are sensitive to both the contour and persistence length of cargo. While the velocity of two couple motors is decreased compared to a single motor (from 531 ± 251 nm/s to as low as 318 ± 287 nm/s), the run length (716 ± 563 nm for a single motor) decreased for short, rigid tethers (to as low as 377 ± 187 μ m) and increased for long, flexible tethers (to as high as 1.74 ± 1.50 μ m). The sensitivity of processive properties to tether rigidity (persistence length) was greatest for short tethers, which caused the motors to exhibit close, yet anti-cooperative coordination. Motors coupled by longer tethers stepped more independently regardless of tether rigidity. Therefore, the properties of the cargo or linkage must play an essential role in motor-motor communication and cargo transport.

1. Introduction

MyoVa is an actin-based, two-headed motor that is well-suited to function as a cargo transporter by virtue of its ability to processively travel long distances (>1 μ m) along actin filaments [1–4]. The importance of intracellular cargo transport is underscored by the fact that mutations in myoVa cause mislocalization and aggregation of cargo such as melanosomes and endoplasmic reticulum in neuronal axons, leading to neurological disorders in humans [5,6]. Upon interaction with an actin filament, the motor domains of myoVa hydrolyze ATP, converting the chemical energy into mechanical motion. When traveling on an actin filament, myoVa exerts a force of ~ 2 pN due to a conformational change in the motor domain [1,7–10]. This small force is sufficient for a tiny motor to transport a large-sized (1 μ m diameter) artificial cargo, such as a plastic or silica bead, on an actin filament in a stepwise manner.

Because of the inherent flexibility of myoVa, the unbound head of

myoVa can undergo a three-dimensional diffusive search and bind to the next binding site on the actin filament during its processive motion [11, 12]. Thus, myoVa can maneuver actin filament intersections by turning at or crossing over actin filament intersections without any reduction in velocity, suggesting its ability to deliver cargo through an actin meshwork [13]. We have previously estimated the flexural stiffness of myoVa subdomains using tethered particle microscopy (TPM) [14]. Interestingly, this analysis showed that full-length myoVa is ~ 5.5 -times less stiff than the lever arm and coiled-coil rod domain, suggesting that the lever arms-rod junction is very flexible; this feature allows the motor to maneuver cargo through the complex actin cytoskeleton [14]. During intracellular cargo transport along the dense actin cytoskeleton, myoVa faces significant physical barriers created by actin-actin intersections, actin-binding proteins, and cellular viscosity. To overcome such physical barriers, multiple motors work together to generate higher forces that depend on the number of motors engaged at any given time and achieve

* Corresponding author. Department of Molecular Physiology and Biophysics, University of Vermont, 149 Beaumont Ave, HSRF 131, Burlington, VT, 05405, USA.

** Corresponding author. Department of Mechanical and Aerospace Engineering, 8 Clarkson Ave, Box 5725, Potsdam NY 13699, USA.

E-mail addresses: ajmichal@clarkson.edu (A.J. Michalek), Yusuf.ali@med.uvm.edu (M.Y. Ali).

<https://doi.org/10.1016/j.bbrep.2021.101194>

Received 23 October 2021; Received in revised form 17 December 2021; Accepted 20 December 2021

2405-5808/© 2021 The Authors. Published by Elsevier B.V. This is an open access article under the CC BY-NC-ND license

(<http://creativecommons.org/licenses/by-nc-nd/4.0/>).

long-distance cargo transport [15,16]. Surprisingly, intracellular cargoes such as melanosomes associate with ~65 bound myoVa molecules, although only a few motors are actively engaged with the actin filament at a given time [17,18]. The mechanism by which motors coordinate within a team and how an individual motor or cargo contributes to collective transport is still unclear. In cells, multiple motors communicate with each other through adapter proteins and cargo, sharing the cytoskeletal resistance among the engaged motors to deliver cargo to its destination. The properties of cargo and the linkage between motors and their cargo must play an essential role in motor-motor communication and cargo transport.

To explore the mechanism of cargo transport by ensembles of molecular motors, researchers have attached multiple motors to non-physiological/physiological cargoes such as Quantum dots, plastic or silica beads, DNA scaffolds, liquid droplets, and liposomes, among others. Experiments using plastic beads have shown that multiple myoVa and kinesin motors cooperate with each other and travel significantly longer distances than a single motor, generating a force that is a multiple of the number of motors [15,16,19]. In contrast, when two kinesin motors are connected using a DNA scaffold, they interfere with each other, generating a force closer to that of a single motor [19]. Similar results have been obtained in cases where two myoVa motors are coupled via a 20-nm diameter Quantum dot or DNA scaffold; in these scenarios, velocity was significantly reduced upon the addition of a second motor, and run-length was moderately increased [20,21]. When multiple kinesins or myoVa motors are attached to a DNA scaffold, the velocity is decreased or remains the same, although the travel distance is significantly increased with increases in motor numbers [22,23]. The ensemble behavior is different in each case because of the diverse elastic properties of cargo and/or linkage between motors. For example, myoVa ensembles move much faster when attached to a very flexible cargo (fluid-like liposome) than when attached to a relatively rigid cargo (gel-like liposome) [24]. Similarly, myoVa ensembles move longer distances with a flexible cargo than with a rigid cargo, although the velocity is the same in both cases [23]. Although considerable effort has been devoted to understanding cargo transport by ensembles of motors, little is known about how the elastic properties of cargo affect the transport process.

Another aspect of cargo transport that is incompletely understood is how motors are organized on the cargo surface and whether the spacing between motors affects cargo transport. Computer simulations suggest that motors are clustered together rather than randomly distributed over the surface of cargo [25]. Such close spacing is expected to enable motors to coordinate with each other. However, a recent study showed that the velocity of dynein with 14-nm spacing was significantly slower than that with 28-nm spacing [26]. In contrast, changing the spacing of multiple kinesin-1 motors does not affect the kinesin-driven motion of microtubules [27]. When a two-myoVa complex travels on an actin filament, the inter-motor distance (distance between heads of motors bound on the actin track) fluctuates, and the trailing motor applies a resistive load on the leading motor that reduces overall speed [20]. This reduction in velocity can be explained by the fact that an external resistive load reduces the velocity of myoVa, whereas an assistive load leaves velocity unchanged.

To better understand how assistive and resistive loads are transmitted between motors by an elastic tether, we constructed a stochastic model of two coupled myoVa motors using Matlab. With stepping kinetics based on experimental measurements, the contour and persistence length of a tether described as a wormlike chain were varied, and predicted velocities and run lengths, along with tether forces, were recorded.

2. Materials and methods

A stochastic model of coupled myoVa dynamics was developed in Matlab (Mathworks Inc, Natick, MA). The model included an actin

filament with a helical pitch of 36 nm and three available binding sites (0 ± 5.14 nm) at each repeat. Each head of two coupled motors was switched between bound and unbound states, with average binding lifetimes governed by tether force (Fig. 1).

When both motors were bound, intermotor distance was defined as the distance between the average location of the heads of the two motors. A wormlike chain model (EQ (1)) was used to calculate, based on intermotor distance (*IMD*), the resistive and assistive forces (F_{tether}) acting on the leading and trailing motor, respectively (Fig. 2, A). The model considered three different tether contour lengths ($L_c = 100$ nm, 150 nm, and 200 nm) along with four different tether persistence lengths ($L_p = 10$ nm, 20 nm, 40 nm, and 80 nm). Physically, the force-extension behavior of the tether accounts for the combined effects of both the motors' tail domains and the cargo connecting them. While simplification of this system to a single, one-dimensional, entropic spring may not accurately represent all physical cargos, it will allow us to independently assess the roles of stepping dynamics (limited by short contour length) and intermotor force (increased by short persistence length) on the ensemble behavior.

$$F_{tether} = \frac{k_B T}{L_p} \left(\frac{IMD}{L_c} + \frac{1}{4 \left(1 - \frac{IMD}{L_c} \right)^2} - \frac{1}{4} \right) \quad [1]$$

Each motor head was assigned a local time clock, which was re-set to zero upon change of state (either from bound to unbound or unbound to bound). Additionally, upon change of state, the head was assigned a random number between zero and one. At each time step, an exponential cumulative distribution function (EQ (2)) is evaluated with inputs of mean lifetime, λ , and local time, t_L . If the value of this function was less than the number assigned to the head, the head state remains unchanged for the next time step. If it was greater, the head state changes, and the head's local clock was re-set. Bound heads are given a mean lifetime which varies based on assistive or resistive load [9] (Fig. 2, B) and is updated at each time step.

$$P = 1 - e^{-\lambda t_L} \quad [2]$$

When a motor's leading head was un-bound, it could either re-bind at the same actin repeat or backstep to the previous one. The transition from unbound to bound was governed by the same process described above for binding lifetime but using a log-normal distribution (EQ (3)) with mean X and standard deviation Y , which were assigned force-independent values of $0.0033 \pm 0.0086s$. These values were calibrated to produce a mean single motor run length of approximately 1500 nm [4,28]. The probability of backstepping was defined as a function of load [9] (Fig. 2, B). Similarly, when a motor's trailing head was un-bound, it could either re-bind at the same actin repeat (stomp) or step forward with probability as a function of load [9] (Fig. 2, B). Additionally, the model prohibited an un-bound head from binding at an actin repeat which already has a bound head (Fig. 1).

$$P = \frac{1}{2} + \frac{1}{2} \left(\frac{\ln t_L - \ln X}{\sqrt{2} Y} \right) \quad [3]$$

For each run, the model was initialized in what was defined as the tumble state, i.e. both heads on one motor were bound and both heads on the other motor were un-bound. The dynamics of the tumble state were governed in much the same manner as stepping, with a local state clock, a random number between zero and one, and a mean \pm SD state lifetime of $0.23 \pm 0.25s$ (see below). The actin repeats available for the tumbling head to land on were assigned probabilities as a function of tether contour length [29].

If, at any time, all four heads switched to an un-bound state the run was terminated. The run length was recorded as the difference between the maximum and minimum head positions. Run time was recorded as the time of termination, and mean velocity was recorded as run length

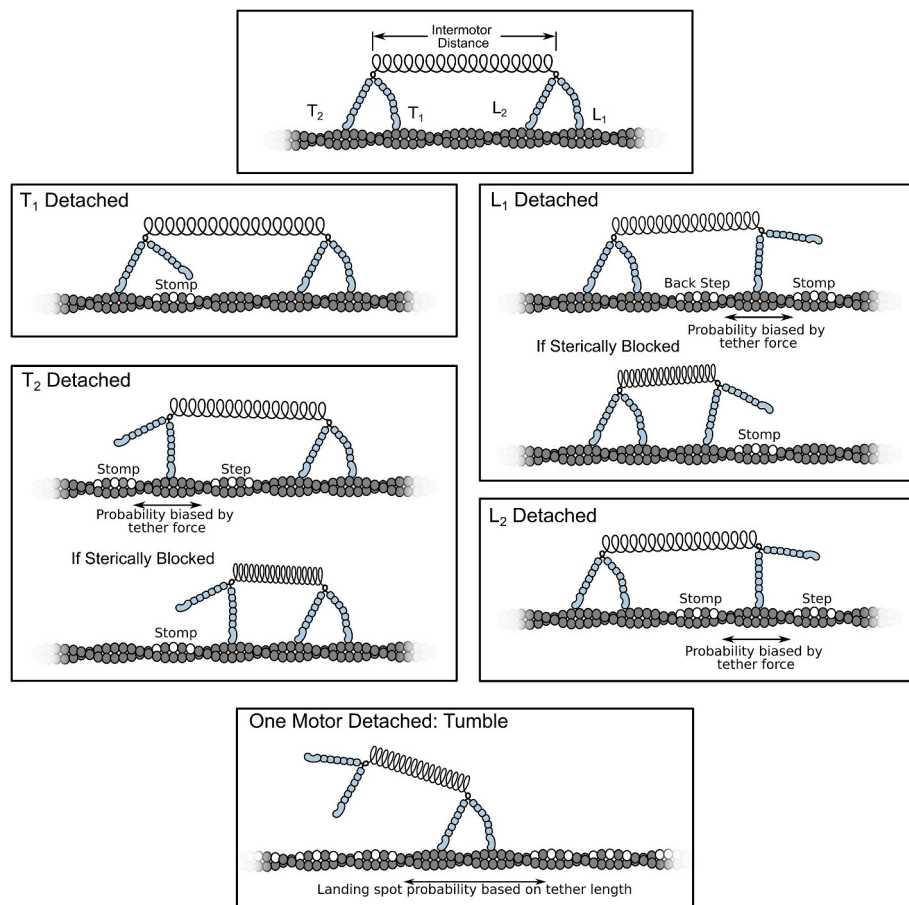


Fig. 1. Schematic representation of possible states described by the model.

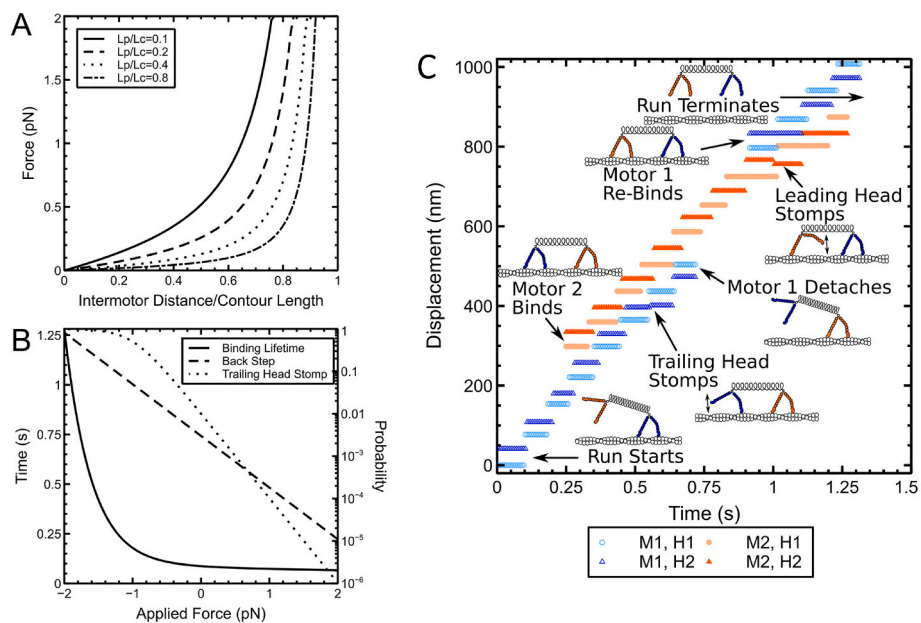


Fig. 2. Tether forces and displacements of two motors. (A) Tether force versus normalized intermotor distance as defined by the wormlike chain model. (B) Mean head binding lifetime and probabilities of leading head backstep or trailing head stomp events as a function of applied force. (C) Representative displacement versus time trace of a two motor complex. Representative processive run, showing various state changes ($L_c = 150$ nm, $L_p = 40$ nm).

divided by run time. For the single motor case, runs over 150 nm in length were compiled for analysis. For tethered cases, runs with lengths more than the tether length plus 50 nm were compiled. These thresholds

were imposed in order to remove from analysis short runs in which velocity calculation may mostly reflect binding of the free motor rather than stepping.

Measurement of attachment time of a motor: When two motor complexes move processively on actin filaments, motors within the complex frequently detach from and reattach to the actin filament. When a labeled motor is detached from the actin track, its stepping pattern becomes noisy and undetectable, distinct from the other motor, which is still bound to the actin filament [20,30]. To calculate the reattachment time of a single motor within the complex, we have counted the number of frames between the detachment from and reattachment to actin track. The number of frames was multiplied by the frame rate, which gives time for attachment time.

3. Results

Processivity (Fig. 2C), with runs longer than the threshold assigned to each case, was seen in 87% of all trials. This included 88% of single motor trials and ranged from 84% ($L_c = 200$ nm, $L_p = 10$ nm) to 91% ($L_c = 100$ nm, $L_p = 80$ nm) of coupled motor trials. Leading motor backstep events were extremely rare, accounting for only 0.0086% of all steps, and were thus not compared between groups.

Both velocity and run length were affected by elastic tether

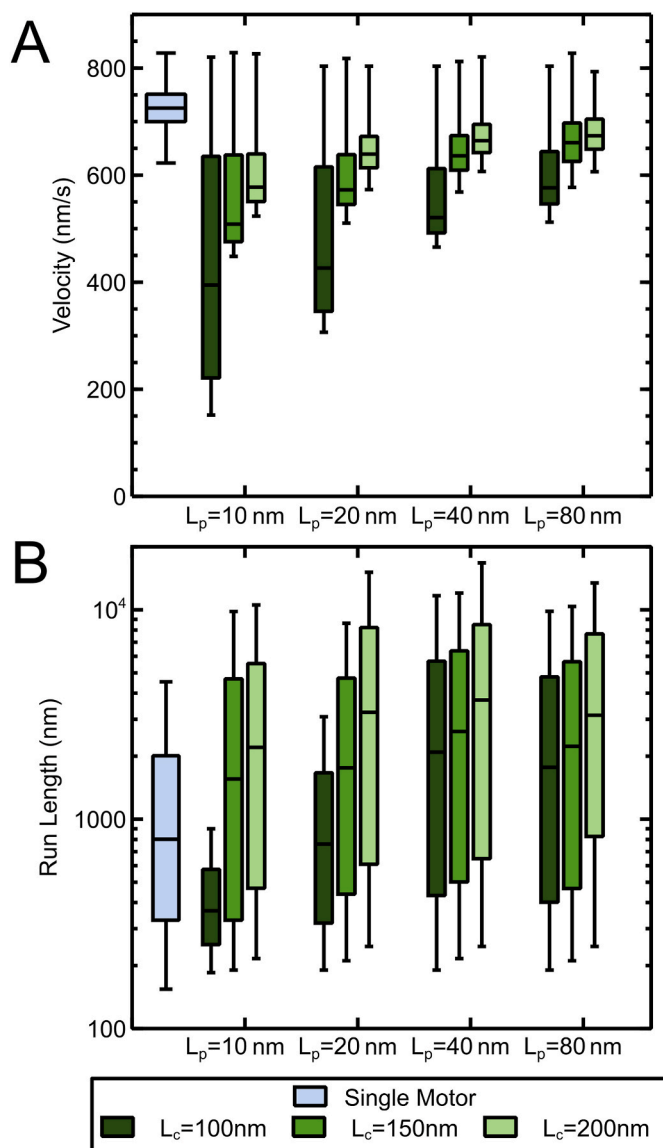


Fig. 3. Velocity and Run length of 1-motor versus 2-motors. (A) Median, quartile, and 95% bounds of average run velocity. (B) Median, quartile, and 95% bounds of run length.

properties (Fig. 3). Mean velocity for a single motor was 531 nm/s, consistent with previously published values ([20,31]. For all combinations of L_c and L_p , mean velocity was decreased relative to that of a single motor (Fig. 3, A). The most rigid tether ($L_c = 100$ nm, $L_p = 10$ nm) resulted in the largest decrease in mean velocity (to 377 nm/s), while the most compliant tether ($L_c = 200$ nm, $L_p = 80$ nm) resulted in the smallest (to 406 nm/s). For a tether or any given persistence length, decreasing contour length decreased both mean and minimum velocity. This effect was largest for lower persistence length (i.e. stiffer) tethers.

The median run length was 717 nm for a single motor, and was longer for two-motor complex than a single motor in most cases (Fig. 3, B). The most compliant tether ($L_c = 200$ nm, $L_p = 80$ nm) resulted in an increase in mean run length to approximately 1700 nm. However, the stiffest tether ($L_c = 100$ nm, $L_p = 10$ nm) resulted in a decrease in mean run length to 377 nm.

Mean tether force decreased with both increasing contour length and increasing persistence length (Fig. 4), ranging from a maximum of 1.262 pN ($L_c = 100$ nm, $L_p = 10$ nm) to a minimum of 0.226 pN ($L_c = 200$ nm, $L_p = 80$ nm). Thus, forces at, or near, the stall force of 2 pN only occurred regularly in 100 nm long tethers.

4. Discussion

We presented a stochastic model of elastically coupled myosin Va motors showing a collective behavior that leads to a longer travel distance (run length) than a single motor on actin filaments (Fig. 3 B). However, the average velocity of two coupled motors is significantly slower than a single motor suggesting that motors are not operating independently but must be mechanically interacting under tension (Fig. 3A). We also establish a model for how the rigidity of cargo influences the overall cargo transport in which both velocity and run length are sensitive to the elastic properties of cargo. In general, velocity decreases, and run-length increases with persistence length and contour length (Fig. 4). Furthermore, we found that the tether force is the highest when the contour (100 nm) and persistence length (10 nm) of cargo was minimum (Fig. 4). Therefore, the communication between motors depends on the stiffness of the cargo and/or the linkage between motor and

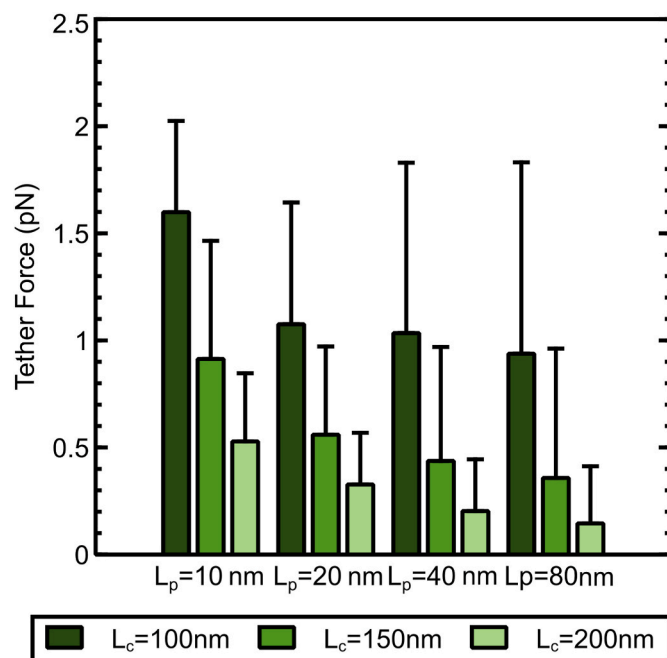


Fig. 4. Tether force depends on the contour length and persistence length. Tether force (Mean \pm SD) decreased with both increasing tether contour length and increasing tether persistence length.

cargo.

While multiple motors transport cargo, they communicate with each other via cargo and adapter proteins. The communication between motors depends on the spatial relationship between motors and the stiffness of the cargo [25,32]. To understand the mechanism of intracellular cargo transport, multiple motors were attached to rigid cargo such as quantum dots (Qdots) [20] or DNA scaffolds [19,21,23] and flexible physiological cargo such as liposomes [24,33]. Interestingly, processive parameters such as velocity, run length, forces of multiple motors were different in each experiment, suggesting that the elastic properties of cargo are sensitive to overall cargo transport. For example, the rigid cargo bound multiple motors move much slower than a single motor [20–22,24], whereas flexible cargo (fluid-state DOPC vesicles) move significantly faster than a single motor [24]. The increased velocity of motors attached to DOPC vesicles, contrary to the decreased velocity of coupled motors predicted by the present work, is likely the result of the vesicles' ability to effectively "roll" along the actin filament as motors detach.

It is predicted that the termination probability of both motors at a given time must be significantly lower than a single motor; therefore, the run length should be many folds longer than a single motor, although speed will remain the same [19,34]. However, consistent with our previously observed experimental data [20,23], we found that velocity was reduced by 40% and 24% for most rigid and most compliant tethers, respectively, while run-length enhancement was only up to 143% for compliant tethers. Thus, we support the idea that due to asynchronized stepping behavior, the tension between motors is built up, leading to negative cooperative behaviors [20,21]. The tension between motors leads to resistive load on the leading motor by the trailing motor, resulting in a slower velocity, backsteps by the leading motor, and force-dependent termination of both motors resulting in moderate enhancement of run length. However, while the probability of a leading motor backstep goes up with tether force, the probability that it will step at all goes down as a result of increased binding lifetime. As a result, under high tether force, the probability that the leading motor will backstep before the trailing motor steps forward (thus reducing the tether force) is extremely low. This highly coordinated stepping can be seen between 0.25s and 0.75s in Fig. 2C. Interestingly, the backsteps are predicted by this model to be significantly less frequent than the 11% that we previously observed [20]. The significantly lower backsteps may imply that the stepping dynamics of elastically coupled motors do not build sufficient tension for taking backsteps. This is consistent with laser trap experiments [9], which showed that the backstep probability is extremely rare at low resistive force (<1 pN, as shown in Fig. 2B) [9], which is the range in which motors attached by more compliant tethers are predicted to spend most of their time. It should also be noted that experiments showing frequent backsteps were performed at sub-saturated ATP (2 μ M), in which binding lifetime is nearly insensitive to assistive or resistive load [1]. Furthermore, myosin Va reacts differentially under assistive and resistive load, as observed in a laser trap experiment [10]. While the speed of a single myosin Va motor is reduced with the resistive load, it remains unaffected under assistive load. Other possibilities for higher backstep probability in our previous experiment [20] include thermal and viscous load being applied to the cargo and geometry between motors to cargo which were not considered in the present stochastic model.

The present model represents the cargo as an entropic spring (wormlike chain) in order to treat tether length (L_c) and stiffness (L_p) independently. Fig. 2, A suggests that some of the tether combinations tested by this model (for example, $L_p = 20$ nm, $L_c = 100$ nm and $L_p = 40$ nm, $L_c = 200$ nm, which both have $L_p/L_c = 0.2$) should have similar elastic properties; however, these combinations result in significantly different processive behavior. In this case, and in similar cases, the combination with the shorter contour length results in lower average tether forces, lower velocities, and shorter run lengths. This is a direct consequence of the motor step size being larger relative to the shorter

tether, which results in rapid increases in tether force when the leading motor steps forward. This phenomenon results in the model prediction that velocity and run length are more sensitive to tether stiffness when the tether is short relative to motor step size than when it is long. As the current model assumes only tensile force in the tether, the effect of compressive force (resulting in assistance of the lead motor and resistance of the trailing motor) remains an important area of future study.

In conclusion, myosin Va motors are attached to a variety of adapter proteins, accessory proteins, and cargo [35–37], and the elastic properties of these proteins are different. Therefore, intracellular cargo transport depends on the properties of motors as well as the properties of adapter proteins and other associated proteins. The result of this stochastic model provides insight into how motors within an ensemble may communicate, cooperate, or even interfere with each other while transporting cargo to their destination, a process critical to the normal functioning of every cell in the human organism.

Declaration of competing interest

The authors declare that they have no conflicting interests.

Data availability

Data will be made available on request.

Acknowledgments

This work was supported by funding from the National Institutes of Health (NIH) grant R03 NS114115. Authors thank Drs. Kathleen Trybus and David Warshaw for allowing them to use the TIRF microscope.

References

- [1] A.D. Mehta, R.S. Rock, M. Rief, J.A. Spudich, M.S. Mooseker, R.E. Cheney, Myosin-V is a processive actin-based motor, *Nature* 400 (1999) 590–593, <https://doi.org/10.1038/23072>.
- [2] D.M. Warshaw, G.G. Kennedy, S.S. Work, E.B. Kremntsova, S. Beck, K.M. Trybus, Differential labeling of myosin V heads with quantum dots allows direct visualization of hand-over-hand processivity, *Biophys. J.* 88 (2005) L30–L32, <https://doi.org/10.1529/biophysj.105.061903>.
- [3] A. Yildiz, J.N. Forkey, S.A. McKinney, T. Ha, Y.E. Goldman, P.R. Selvin, Myosin V walks hand-over-hand: single fluorophore imaging with 1.5-nm localization, *Science* 300 (2003) 2061–2065, <https://doi.org/10.1126/science.1084398>.
- [4] M.Y. Ali, S. Uemura, K. Adachi, H. Itoh, K. Kinoshita Jr., S. Ishiwata, Myosin V is a left-handed spiral motor on the right-handed actin helix, *Nat. Struct. Biol.* 9 (2002) 464–467, <https://doi.org/10.1038/nsb803>.
- [5] W. Wagner, S.D. Brenowitz, J.A. Hammer 3rd, Myosin-Va transports the endoplasmic reticulum into the dendritic spines of Purkinje neurons, *Nat. Cell Biol.* 13 (2011) 40–48, <https://doi.org/10.1038/ncb2132>.
- [6] E. Pastural, F.J. Barrat, R. Dufourcq-Lagelouse, S. Certain, O. Sanal, N. Jabado, R. Seger, C. Griscelli, A. Fischer, G. de Saint Basile, Griscelli disease maps to chromosome 15q21 and is associated with mutations in the myosin-Va gene, *Nat. Genet.* 16 (1997) 289–292, <https://doi.org/10.1038/ng0797-289>.
- [7] C. Veigel, F. Wang, M.L. Bartoo, J.R. Sellers, J.E. Molloy, The gated gait of the processive molecular motor, myosin V, *Nat. Cell Biol.* 4 (2002) 59–65, <https://doi.org/10.1038/ncb732>.
- [8] S. Uemura, H. Higuchi, A.O. Olivares, E.M. De La Cruz, S. Ishiwata, Mechanochemical coupling of two substeps in a single myosin V motor, *Nat. Struct. Mol. Biol.* 11 (2004) 877–883, <https://doi.org/10.1038/nsmb806>.
- [9] N.M. Kad, K.M. Trybus, D.M. Warshaw, Load and Pi control flux through the branched kinetic cycle of myosin V, *J. Biol. Chem.* 283 (2008) 17477–17484, <https://doi.org/10.1074/jbc.M800539200>.
- [10] J.C. Gebhardt, A.E. Clemen, J. Jaud, M. Rief, Myosin-V is a mechanical ratchet, *Proc. Natl. Acad. Sci. U. S. A.* 103 (2006) 8680–8685, <https://doi.org/10.1073/pnas.0510191103>.
- [11] A.R. Dunn, J.A. Spudich, Dynamics of the unbound head during myosin V processive translocation, *Nat. Struct. Mol. Biol.* 14 (2007) 246–248, <https://doi.org/10.1038/nsmb1206>.
- [12] K. Shiroguchi, K. Kinoshita Jr., Myosin V walks by lever action and Brownian motion, *Science* 316 (2007) 1208–1212, <https://doi.org/10.1126/science.1140468>.
- [13] M.Y. Ali, E.B. Kremntsova, G.G. Kennedy, R. Mahaffy, T.D. Pollard, K.M. Trybus, D.M. Warshaw, Myosin Va maneuvers through actin intersections and diffuses along microtubules, *Proc. Natl. Acad. Sci. U. S. A.* 104 (2007) 4332–4336, <https://doi.org/10.1073/pnas.0611471104>.

- [14] A.J. Michalek, G.G. Kennedy, D.M. Warshaw, M.Y. Ali, Flexural stiffness of myosin Va subdomains as measured from tethered particle motion, *J Biophys* 2015 (2015) 465693, <https://doi.org/10.1155/2015/465693>.
- [15] H.W. Schroeder 3rd, C. Mitchell, H. Shuman, E.L. Holzbaur, Y.E. Goldman, Motor number controls cargo switching at actin-microtubule intersections in vitro, *Curr. Biol.* 20 (2010) 687–696, <https://doi.org/10.1016/j.cub.2010.03.024>.
- [16] M. Vershinin, B.C. Carter, D.S. Razafsky, S.J. King, S.P. Gross, Multiple-motor based transport and its regulation by Tau, *Proc. Natl. Acad. Sci. U. S. A.* 104 (2007) 87–92, <https://doi.org/10.1073/pnas.0607919104>.
- [17] S.P. Gross, M.C. Tuma, S.W. Deacon, A.S. Serpinskaya, A.R. Reilein, V.I. Gelfand, Interactions and regulation of molecular motors in *Xenopus melanophores*, *J. Cell Biol.* 156 (2002) 855–865, <https://doi.org/10.1083/jcb.200105055>.
- [18] E.L. Holzbaur, Y.E. Goldman, Coordination of molecular motors: from in vitro assays to intracellular dynamics, *Curr. Opin. Cell Biol.* 22 (2010) 4–13, <https://doi.org/10.1016/j.ceb.2009.12.014>.
- [19] A.R. Rogers, J.W. Driver, P.E. Constantinou, D. Kenneth Jamison, M.R. Diehl, Negative interference dominates collective transport of kinesin motors in the absence of load, *Phys. Chem. Chem. Phys.* 11 (2009) 4882–4889, <https://doi.org/10.1039/b900964g>.
- [20] M.Y. Ali, A. Vilfan, K.M. Trybus, D.M. Warshaw, Cargo transport by two coupled myosin Va motors on actin filaments and bundles, *Biophys. J.* 111 (2016) 2228–2240, <https://doi.org/10.1016/j.bpj.2016.09.046>.
- [21] H. Lu, A.K. Efremov, C.S. Bookwalter, E.B. Kremntsova, J.W. Driver, K.M. Trybus, M.R. Diehl, Collective dynamics of elastically coupled myosin V motors, *J. Biol. Chem.* 287 (2012) 27753–27761, <https://doi.org/10.1074/jbc.M112.371393>.
- [22] K. Furuta, A. Furuta, Y.Y. Toyoshima, M. Amino, K. Oiwa, H. Kojima, Measuring collective transport by defined numbers of processive and nonprocessive kinesin motors, *Proc. Natl. Acad. Sci. U. S. A.* 110 (2013) 501–506, <https://doi.org/10.1073/pnas.1201390110>.
- [23] E.B. Kremntsova, K. Furuta, K. Oiwa, K.M. Trybus, M.Y. Ali, Small teams of myosin Vc motors coordinate their stepping for efficient cargo transport on actin bundles, *J. Biol. Chem.* 292 (2017) 10998–11008, <https://doi.org/10.1074/jbc.M117.780791>.
- [24] S.R. Nelson, M.Y. Ali, K.M. Trybus, D.M. Warshaw, Random walk of processive, quantum dot-labeled myosin Va molecules within the actin cortex of COS-7 cells, *Biophys. J.* 97 (2009) 509–518, <https://doi.org/10.1016/j.bpj.2009.04.052>.
- [25] R.P. Erickson, Z. Jia, S.P. Gross, C.C. Yu, How molecular motors are arranged on a cargo is important for vesicular transport, *PLoS Comput. Biol.* 7 (2011), e1002032, <https://doi.org/10.1371/journal.pcbi.1002032>.
- [26] R. Ibusuki, M. Shiraga, A. Furuta, M. Yoshio, H. Kojima, K. Oiwa, K. Furuta, Collective motility of dynein linear arrays built on DNA nanotubes, *Biochem. Biophys. Res. Commun.* 523 (2020) 1014–1019, <https://doi.org/10.1016/j.bbrc.2019.12.125>.
- [27] T. Kaneko, S. Ando, K. Furuta, K. Oiwa, H. Shintaku, H. Kotera, R. Yokokawa, Transport of microtubules according to the number and spacing of kinesin motors on gold nano-pillars, *Nanoscale* 11 (2019) 9879–9887, <https://doi.org/10.1039/c9nr01324e>.
- [28] T. Sakamoto, I. Amitani, E. Yokota, T. Ando, Direct observation of processive movement by individual myosin V molecules, *Biochem. Biophys. Res. Commun.* 272 (2000) 586–590, <https://doi.org/10.1006/bbrc.2000.2819>.
- [29] P.C. Nelson, C. Zurla, D. Brogioli, J.F. Beausang, L. Finzi, D. Dunlap, Tethered particle motion as a diagnostic of DNA tether length, *J. Phys. Chem. B* 110 (2006) 17260–17267, <https://doi.org/10.1021/jp0630673>.
- [30] M.Y. Ali, G.G. Kennedy, D. Safer, K.M. Trybus, H.L. Sweeney, D.M. Warshaw, Myosin Va and myosin VI coordinate their steps while engaged in an in vitro tug of war during cargo transport, *Proc. Natl. Acad. Sci. U. S. A.* 108 (2011) E535–E541, <https://doi.org/10.1073/pnas.1104298108>.
- [31] J.M. Armstrong, E. Kremntsova, A.J. Michalek, A.T. Heaslip, S.R. Nelson, K. M. Trybus, D.M. Warshaw, Full-length myosin Va exhibits altered gating during processive movement on actin, *Proc. Natl. Acad. Sci. U. S. A.* 109 (2012) E218–E224, <https://doi.org/10.1073/pnas.1109709109>.
- [32] F. Berger, C. Keller, S. Klumpp, R. Lipowsky, External forces influence the elastic coupling effects during cargo transport by molecular motors, *Phys. Rev. E - Stat. Nonlinear Soft Matter Phys.* 91 (2015), 022701, <https://doi.org/10.1103/PhysRevE.91.022701>.
- [33] A.T. Lombardo, S.R. Nelson, M.Y. Ali, G.G. Kennedy, K.M. Trybus, S. Walcott, D. M. Warshaw, Myosin Va molecular motors manoeuvre liposome cargo through suspended actin filament intersections in vitro, *Nat. Commun.* 8 (2017) 15692, <https://doi.org/10.1038/ncomms15692>.
- [34] G.T. Shubeita, S.L. Tran, J. Xu, M. Vershinin, S. Cermelli, S.L. Cotton, M.A. Welte, S.P. Gross, Consequences of motor copy number on the intracellular transport of kinesin-1-driven lipid droplets, *Cell* 135 (2008) 1098–1107, <https://doi.org/10.1016/j.cell.2008.10.021>.
- [35] I. Rojo Pulido, T.D. Nightingale, F. Darchen, M.C. Seabra, D.F. Cutler, V. Gerke, Myosin Va acts in concert with Rab27a and MyRIP to regulate acute von-Willebrand factor release from endothelial cells, *Traffic* 12 (2011) 1371–1382, <https://doi.org/10.1111/j.1600-0854.2011.01248.x>.
- [36] F. Brozzi, F. Diraison, S. Lajus, S. Rajatileka, T. Philips, R. Regazzi, M. Fukuda, P. Verkade, E. Molnar, A. Varadi, Molecular mechanism of myosin Va recruitment to dense core secretory granules, *Traffic* 13 (2012) 54–69, <https://doi.org/10.1111/j.1600-0854.2011.01301.x>.
- [37] C. Desnos, J.S. Schonn, S. Huet, V.S. Tran, A. El-Amraoui, G. Raposo, I. Fanget, C. Chapuis, G. Menasche, G. de Saint Basile, C. Petit, S. Cribier, J.P. Henry, F. Darchen, Rab27A and its effector MyRIP link secretory granules to F-actin and control their motion towards release sites, *J. Cell Biol.* 163 (2003) 559–570, <https://doi.org/10.1083/jcb.200302157>.